FULL PAPER

Rational design of Pt-Pd-Ni trimetallic nanocatalysts for room temperature benzaldehyde and styrene hydrogenation

Tuo Zheng,[b] Fengshun Wu,[b] Huan Fu,[b] Li Zeng,[b] Congxiao Shang, [a, c] Lihua Zhu,*[a, b] and Zhengxiao Guo*[a, c]

Abstract: Multimetallic nanostructures offer great scope for fine tuning of heterogeneous catalysis, but clear understanding of surface chemistry and structure is important to enhance selectivity and efficiency. Focussing on a Pt-Pd-Ni trimetallic system, we comparatively examined the Ni/C, Pt/Ni/C, Pd/Ni/C and Pt-Pd/Ni/C catalysts synthesized by galvanic replacement reaction at room temperature. To clarify surface chemical/structural effect, the Pt-Pd/Ni/C-X catalyst was thermally treated at X = 200, 400 or 600 °C in a H_2 reducing atmosphere. The as-prepared catalysts were characterized by XRD, XPS, TEM, HRTEM, HS-LEIS and STEM-EDS elemental mapping and line-scanning. All the catalysts are comparatively evaluated for benzaldehyde and styrene hydrogenation. It is shown that PtPd alloy nanoclusters, a nanostructure with "PtPd alloy nanoclusters on Ni nanoparticles" (PtPd/Ni) and the synergistic effect of Pt-Pd and Ni, lead to much improved catalytic performance of Pt-Pd/Ni/C, compared with the monometallic or bimetallic counterparts. With the increase of the treatment temperature of the Pt-Pd/Ni/C-X, the catalytic property is gradually reduced, which is likely due to that the favourable nanostructure of fine "PtPd/Ni" is gradually transformed to relatively large "PtPdNi alloy on Ni" (PtPdNi/Ni) particles, thus decreasing the number of noble metal (Pt and Pd) active sites on the surface of the catalyst.

Introduction

Metal-based nanostructures are widely used for heterogeneous catalysis, such as oxidation, hydrogenation and electrocatalysis. The catalysts have gradually evolved from monometallic to multimetallic structures. Particularly, multimetallic catalysts containing precious metals can significantly reduce the amount of noble metals and simultaneously improve their catalytic performance (activity, selectivity and stability), due to synergetic effect among related species,[1-19] For instance, a small amount of Rh was added to a Pt-based catalyst, forming a Pt-Rh bimetallic system, its stability for the catalytic oxidation of ammonia was markedly improved.[20] The Au/SiO_2 (hereafter, "/" stands for "supported on"), Au/ZrO_2, Au/TiO_2, Au/ZnO monometallic catalysts and Au-In/ZnO bimetallic supported catalysts were prepared by Claus *et al.*, [21,22] and were applied in selective hydrogenation of acrolein. The selectivity of the Au-In/ZnO catalyst for C=O double bond hydrogenation was greater than that of the other catalysts. A $Ru/Ni/Ni(OH)_2/C$ catalyst was successfully synthesized at room temperature by hydrazine hydrate reduction and galvanic replacement strategies, [23] and the catalyst shows higher selectivity to decalin and activity for hydrogenation of naphthalene than those of $Ni/Ni(OH)_2/C$, Ru-Ni/C and Ru/C due to the synergistic effect of Ru, Ni and $Ni(OH)_2$.[23] However, the specific mechanism of the synergistic effect in the multimetallic catalysts needs further clarification in order to make full use of such effect. In addition, the majority of the literature in heterogeneous catalytic hydrogenation is focused on the monometallic and bimetallic catalysts, and relevant studies on trimetallic systems are still lacking. Therefore, it is of both fundamental and practical importance to explore the synergistic effect of the trimetallic catalysts in catalytic hydrogenation.

The catalytic properties of the multimetallic catalysts are directly determined by their surface chemistry and structure,[24-28] which can be tailored by different methods, e.g. thermal treatment, to regulate their catalytic performance. For instance, Au_nPt_{100-n} nanoparticles were prepared by Zhong *et al.*[29] After modification in a reducing atmosphere of 15%H_2, those Au_nPt_{100-n} exist in the form of a relatively uniform alloy after treatment around 300-400 °C, but show a Pt@Au core-shell or phase-separated structure with Au-rich surface or particles if the treatment temperature is relatively high (e.g. 800 °C). It was also found that the catalytic properties of the Au_nPt_{100-n} alloy are superior to those of the Au@Pt and Au-Pt phase-separated structure for oxygen reduction reaction (ORR) reaction. In one of our previous studies, the nanostructures of the RuNiCo/C (or RuNi/C) catalysts were successfully modified by change of the reduction temperature, and the relationship between their nanostructures and catalytic naphthalene hydrogenation (or benzene hydrogenation) performance is established.[30, 31]

In view of the above, the thermal treatment of a Pt-Pd/Ni/C-X (X stands for the treatment temperature) in H_2 was investigated here to improve its catalytic performance for benzaldehyde (or styrene) hydrogenation. The monometallic (Ni/C), bimetallic (Pt/Ni/C, Pd/Ni/C) and trimetallic (Pt-Pd/Ni/C) catalysts were synthesized, and the hydrogenation of benzaldehyde (or styrene) was used as probe reaction. Their catalytic properties were compared and the reasons for the difference were elucidated. The synergistic effect in the Pt-Pd/Ni/C catalyst was investigated. The relationship between the annealing temperature of Pt-Pd/Ni/C-X and its catalytic hydrogenation performance was explored. This study provides fundamental support to the design and synthesis of highly efficient and low-cost multimetallic nanocatalysts for hydrogenation reactions.

[a] *Dr. L. Zhu, Dr. C. Shang, Prof. Dr. ZX. Guo*
Department of Chemistry, The University of Hong Kong, Hong Kong SAR, China
E-mail: zxguo@hku.hk
[b] *T. Zheng, F. Wu, H. Fu, L. Zeng, Dr. L. Zhu*
College of Chemistry and Chemical Engineering, Faculty of Materials Metallurgy and Chemistry, Jiangxi University of Science and Technology, Ganzhou 341000, Jiang Xi, China
E-mail: zhulihua@163.com; Tel: +86-979-8312204
[c] *Dr. C. Shang , Prof. Dr. ZX. Guo, Zhejiang Institute of Research and Innovation, The University of Hong Kong, Hangzhou, China*
E-mail: zxguo@hku.hk.

Results and Discussion

XRD characterization of the catalysts

Figure 1 shows the XRD patterns of Pt/Ni/C, Pd/Ni/C and Pt-Pd/Ni/C and Pt-Pd/Ni/C-X catalysts. For the Pt/Ni/C, Pd/Ni/C and Pt-Pd/Ni/C catalysts, the diffraction peaks at 2θ = 44.5°, 51.8° and 76.4° belong to Ni (111), (200) and (220) planes, respectively (Figure 1A),[32, 33] indicating that the nickel crystallites exist in these catalysts. In the XRD patterns of Pt/Ni/C, there is a weak diffraction peak of PtNi(111) alloy (2θ = 42.8°). For Pd/Ni/C, a weak diffraction peak of Pd(111) plane appears at 40.1°.[34-36] In the XRD patterns of Pt-Pd/Ni/C, the diffraction peak at 2θ = 40° is assigned to PtPd(111) alloy phase. The results show that the presence of Pt leads to the formation of an PtPd alloy. The nanostructure of the Pt-Pd/Ni/C catalyst is likely to be PtPd alloy-supported on Ni nanoparticle. When the reducing temperature of Pt-Pd/Ni/C increased from 200 to 600 °C, a PtPdNi(111) trimetallic alloy was formed (Figure 1B). Hence, the Pt-Pd/Ni/C-600 catalyst possesses a structure of PtPdNi alloy nanoclusters loaded on Ni nanoparticles.

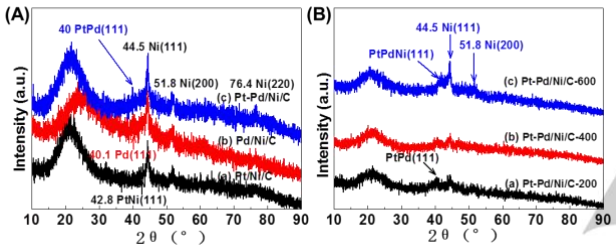

Figure 1. XRD patterns of the catalysts (A) (a) Pt/Ni/C, (b) Pd/Ni/C and (c) Pt-Pd/Ni/C; (B) (a) Pt-Pd/Ni/C-200, (b) Pt-Pd/Ni/C-400 and (c) Pt-Pd/Ni/C-600.

XPS characterization of the catalysts

In order to clarify the chemical states of the different species and their corresponding concentrations on the surface of the catalysts, XPS was conducted on Ni/C, Pt/Ni/C, Pd/Ni/C and Pt-Pd/Ni/C and Pt-Pd/Ni/C-600 catalysts. The results are shown in Figures 2 and 3. The peak area of NiOOH(857.1 eV), $Ni(OH)_2$(855.4 eV), NiO(853.9 eV) and Ni(0)(852.7 eV) on the surface of the catalysts was compared. It was found that the main Ni species was oxidized. This is somewhat expected, as surface Ni(0) readily reacts with oxygen and water in air, particularly in nano-scale particles.

Figure 3 shows the XPS spectra of Pt 4f and Pd 3d for Pt/Ni/C, Pd/Ni/C and Pt-Pd/Ni/C and Pt-Pd/Ni/C-600 catalysts. It can be seen that the Pt species mainly exist in the form of Pt^{2+}(72.4 eV), Pt^{4+}(73.5 eV) and Pt(0)(71.5 eV) on the surface of the Pt/Ni/C and Pt-Pd/Ni/C catalysts. However, the Pd species on the surface of the Pd/Ni/C and Pt-Pd/Ni/C catalysts are mainly in the form of Pd(0)(335.6 eV), with a small amount of oxidized Pd^{n+} species (337.5 eV) [42]. The possible reason is that the dispersion of Pt on the catalyst surface is much higher than that of Pd, which makes the surface Pt species more susceptible to oxidization (relative to Pd species). Particularly, most Pd species on the surface of Pt-Pd/Ni/C are in the form of the reduction state, which is probably due to the formation of PtPd alloy nanoclusters. PtPd alloy further prevents Pd from being oxidized. The Pt (Pd) specie on the surface of the Pt-Pd/Ni/C-600 catalyst is mainly Pt(0) (Pd(0)) due to the existence of PtPdNi trimetallic nano-alloy, which can largely protect Pt(0) and Pd(0) from being oxidized.

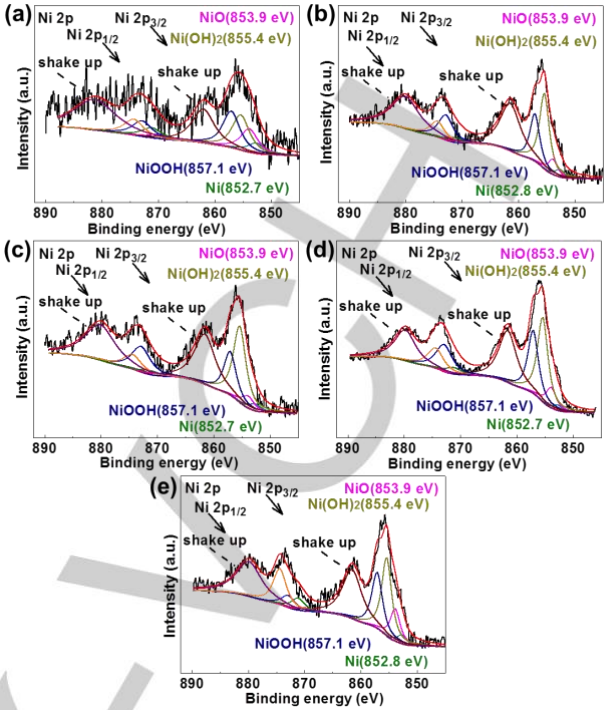

Figure 2. Ni 2p XPS spectra of the catalysts: (a) Ni/C, (b) Pt/Ni/C, (c) Pd/Ni/C, (d) Pt-Pd/Ni/C and (e) Pt-Pd/Ni/C-600.

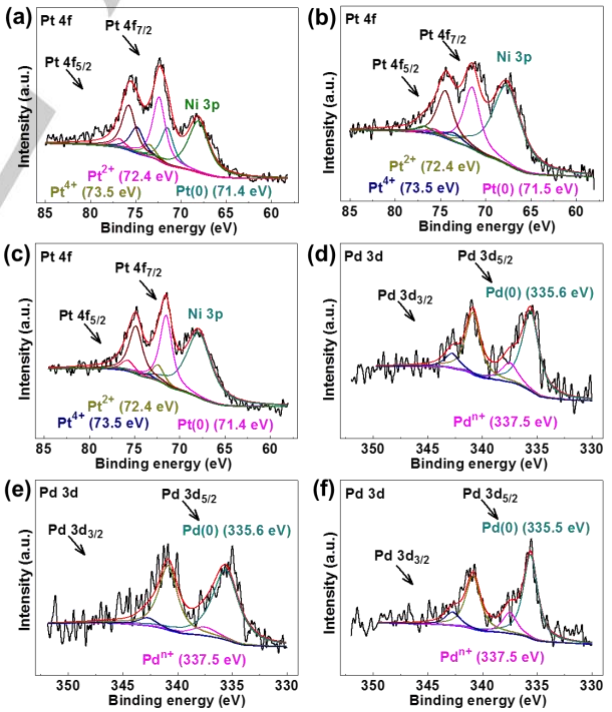

Figure 3. Pt 4f XPS spectra of (a) Pt/Ni/C, (b) Pt-Pd/Ni/C and (c) Pt-Pd/Ni/C-600 and Pd 3d XPS spectra of (d) Pd/Ni/C, (e) Pt-Pd/Ni/C and (f) Pt-Pd/Ni/C-600.

TEM and HRTEM characterization of the catalysts

TEM images and particle size distribution of the Pt-Pd/Ni nanoparticles in the Pt-Pd/Ni/C and Pt-Pd/Ni/C-600 catalysts are given (Figure 4). It can be seen that the size distribution of Pt-Pd/Ni particles in the Pt-Pd/Ni/c catalyst is between 1 and 25 nm. The average particle size was calculated to be 7.79 nm using the Sigmascan software. There is no agglomeration of the nanoparticles. As the reducing temperature of Pt-Pd/Ni/C increases from 300 to 600 °C, the Pt-Pd/Ni/C nanoparticles grow to an average size of 14.08 nm.

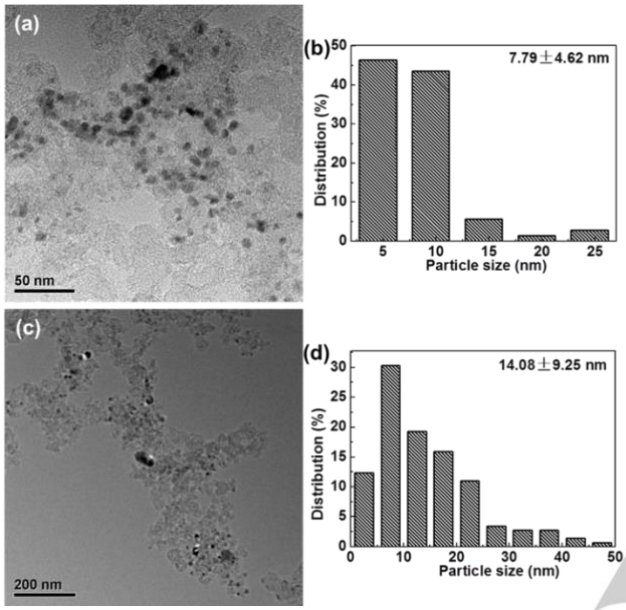

Figure 4. (a) TEM images and Pt-Pd/Ni nanoparticles size distribution for (a, b) Pt-Pd/Ni/C and (c, d) Pt-Pd/Ni/C-600 catalysts.

The TEM and HRTEM images of the Pt-Pd/Ni/C catalyst are shown in Figure 5. Most particles are less than 20 nm in size and are uniformly distributed. In the HRTEM of the catalyst, the lattice fringes are with a distance of 0.203 and 0.225 nm. According to JCPDS card No. 04-0850, 0.203 nm is corresponding to the crystal plane of Ni(111). The distance of 0.225 nm is between 0.224 nm (Pd(111)) (Pd-JCPDS card No. 65-2867) and 0.226 nm (Pt(111)) (Pt-JCPDS card No. 65-2868), which is assigned to the crystal plane of PtPd alloy(111). The XRD and XPS results indicate clearly that the Pt-Pd/Ni structure in the Pt-Pd/Ni/C catalyst consists of PtPd alloy nanoclusters supported on Ni nanoparticles. This is probably the main reason for the superior catalytic performance of the Pt-Pd/Ni/C catalyst, compared to the Pt/Ni/C and Pd/Ni/C catalysts, for benzaldehyde (or styrene) hydrogenation reaction (Tables 1 and 2).

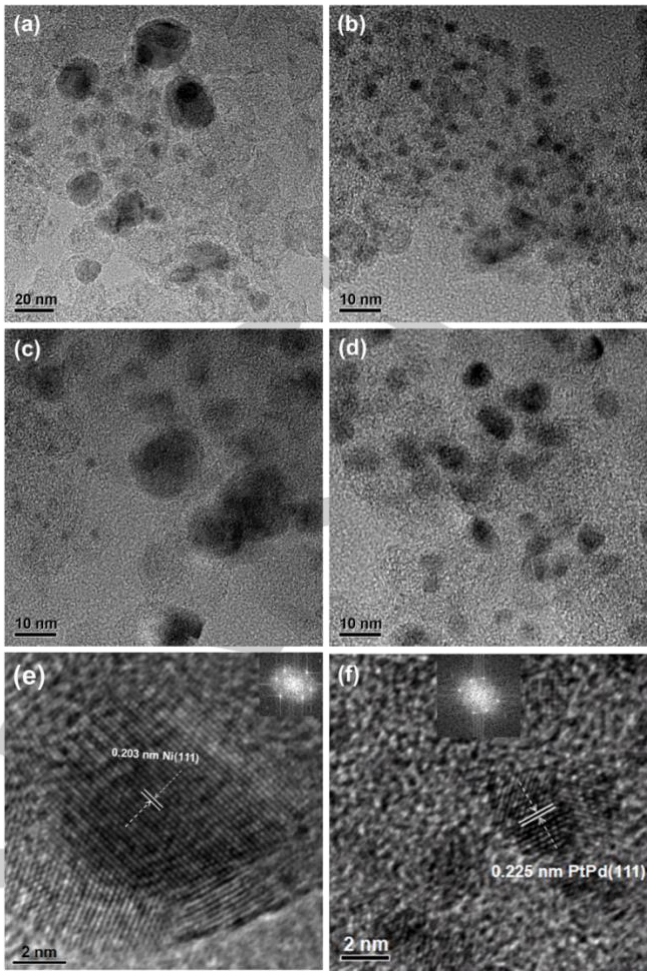

Figure 5. (a, b) TEM and (c-f) HRTEM images of the Pt-Pd/Ni/C catalyst.

Figure 6 is the HRTEM image of the Pt-Pd/Ni/C-600 catalyst. The lattice fringes with a spacing of 0.203 nm can be ascribed to the Ni(111) facet (JCPDS card No. 04-0850). The lattice fringes with a spacing of 0.225 nm in Figure 6 (b) are attributed to the PtPdNi alloy (111) (compared with Pd(111) = 0.224 nm; Pt(111) = 0.226 nm). On the basis of the above XRD and XPS results, we can conclude that a PtPdNi trimetallic alloy is gradually formed when the annealing temperature is increased to 600 °C. There are no PtPd alloy nanoclusters. Therefore, the surface structure of the Pt-Pd/Ni/C-600 catalyst mainly consists of PtPdNi alloy nanoclusters supported on Ni nanoparticles.

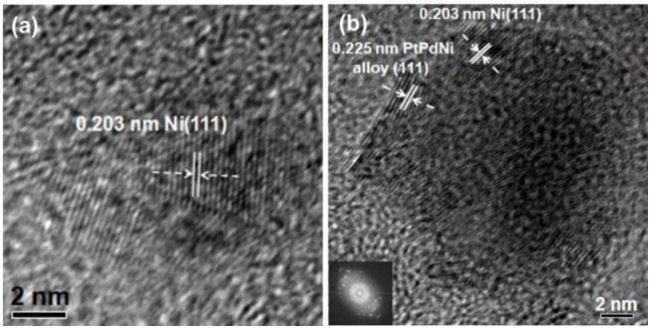

Figure 6. (a, b) HRTEM images of Pt-Pd/Ni/C-600 catalyst.

HAADF-STEM images, STEM-EDS elemental-mapping and line-scanning of the catalysts

In order to further identify the difference of the nanostructures between the Pt-Pd/Ni/C and the Pt-Pd/Ni/C-600 catalysts, the HAADF-STEM (High-Angle Annular Dark-Field imaging – Scanning Transmission Electron Microscopy), STEM-EDS (Energy Dispersive Spectroscopy) elemental mapping scanning and line-scanning were used to characterize the catalysts. The results are shown in Figures 7 and 8. HAADF-STEM images show that the Pt-Pd/Ni in the Pt-Pd/Ni/C catalyst is less than 20 nm, highly dispersed and without agglomeration, which is in good agreement with TEM results. The results show that Ni, Pd and Pt together exist, and the distribution of Ni element do not overlap with that of Pd or Pt, but the distribution of Pd completely overlaps with that of Pt. In addition, the results of an elemental line-scanning of a representative nanoparticle show that the intensity fluctuations of Pd and Pt coincide well with each other, but do not math that of Ni. The above results strongly indicate that PtPd alloy nanoclusters are formed in the Pt-Pd/Ni/C catalyst, but the PtPd alloy nanoclusters are phase segregated from the Ni (maybe PtPd-on-Ni). Together with other analysis results, we can propose that a "PtPd alloy nanocluster-on-Ni nanoparticle" nanostructure has been formed in the Pt-Pd/Ni/C catalyst.

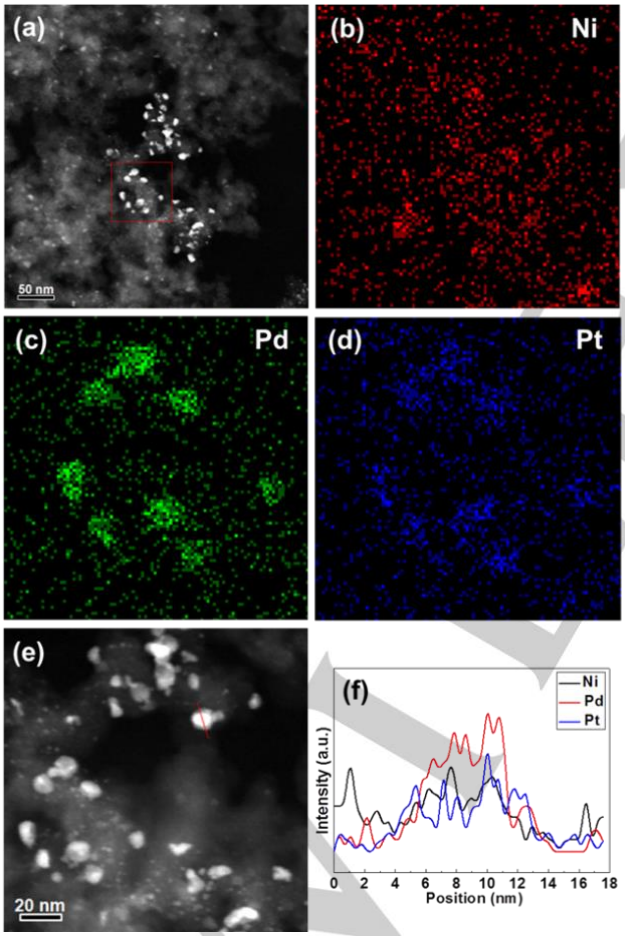

Figure 7. (a, e) HAADF-STEM image, (b-d) STEM-EDS elemental mapping, Ni (red), Pd (green), Pt (blue) and (f) line-scanning results of the Pt-Pd/Ni/C catalyst.

Figure 8 shows the HAADF-STEM images of the Pt-Pd/Ni/C-600 catalyst and the corresponding STEM-EDS elemental mapping and line-scanning results. The results suggest that the intensity of Ni signal is much higher than that of Pt and Pd, and Ni, Pt and Pd are all present in each nanoparticle. The Pt and Pd show similar intensities. The results of elemental line scan of Pt-Pd/Ni/C-600 catalyst nanoparticles are consistent with the results of elemental surface scan. The intensity of Ni is clearly much higher than that of Pt and Pd, and the distribution and location of Pt are in accord with that of Pd. The results indicate that the Pt-Pd/Ni/C-600 catalyst is characterised by "PtPdNi alloy nanoclusters on Ni nanoparticles".

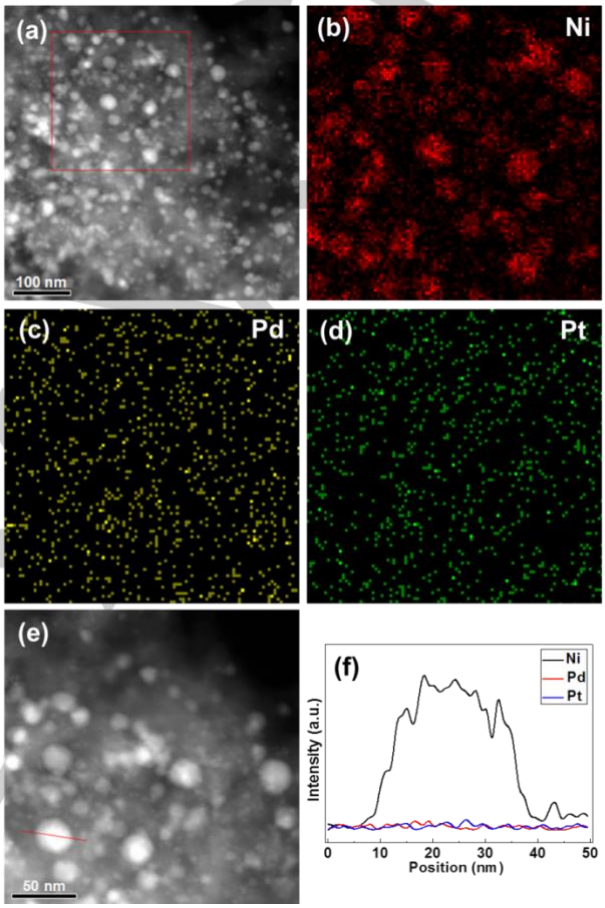

Figure 8. (a, e) HAADF-STEM image, (b-d) STEM-EDS elemental mapping, Ni (red), Pd (yellow), Pt (blue) and (f) line-scanning results of the Pt-Pd/Ni/C-600 catalyst.

HS-LEIS characterization of the catalysts

In order to study the difference of the types and contents of atoms on the surface of the catalysts, the Ni/C, Pt/Ni/C, Pd/Ni/C, Pt-Pd/Ni/C and Pt-Pd/Ni/C-600 catalysts were characterized by High-Sensitivity Low-Energy Ion Scattering (HS-LEIS) with 5 keV $^{20}Ne^{+}$ ions as scattering source, respectively. The HS-LEIS spectra are shown in Figure 9. The signal of Ni peak can be seen in the HS-LEIS spectra of Ni/C, Pt/Ni/C, Pd/Ni/C, Pt-Pd/Ni/C and Pt-Pd/Ni/C-600 catalysts. In the HS-LEIS spectra of Pt/Ni/C, Pt-Pd/Ni/C and Pt-Pd/Ni/C-600, the weak signal of the Pt peak is observed. However, in the HS-LEIS spectra of Pd/Ni/C, Pt-Pd/Ni/C and Pt-Pd/Ni/C-600, the intensity of the Pd peak is much higher than that of the Pt peak. This indicates that the concentration of Pd is much greater than that of Pt on the outmost surface of the Pt-Pd/Ni/C and Pt-Pd/Ni/C-600 catalysts. The concentration of Ni on the outer surface of the bimetallic and trimetallic catalysts is higher

than that of other elements. The reason for the above is that Pt and Ni are more compatible than Pd and Ni. Then the Pt atoms tend to locate on the surface of Ni atoms, but the Pd atoms easily move to the surface of Pt-Pd/Ni, forming segregation. As a result, the intensity of Pd is much larger than that of Pt on the outmost surface of Pt-Pd/Ni/C. The intensity of Pd on the outer surface of the Pd/Ni/C is evidently higher than that of Pt on the outmost surface of the Pt/Ni/C due to ready accumulation of Pd on the surface. Moreover, comparison of the HS-LEIS spectra of Pt-Pd/Ni/C with that of the Pd/Ni/C indicates that the intensity of Pd in the Pt-Pd/Ni/C is much lower than that in Pd/Ni/C because the formation of PtPd alloy reduces the amount of Pd on the surface. Moreover, the Ni/(Pd+Pt) atomic ratio for the Pt-Pd/Ni/C-600 is lower than that for the Pt-Pd/Ni/C due to the presence of the PtPdNi alloy nanoclusters in the Pt-Pd/Ni/C-600 catalyst. These HS-LEIS results further prove the exact nanostructures in the Pt-Pd/Ni/C (PtPd alloy-on-Ni) and Pt-Pd/Ni/C-600 (PtPdNi alloy-on-Ni) catalysts.

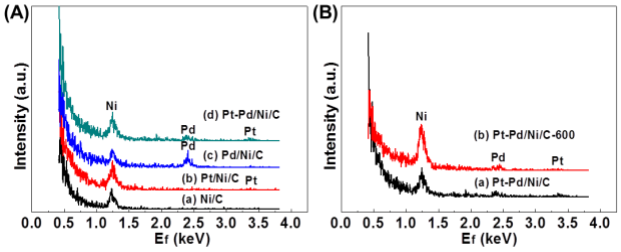

Figure 9. (A, B) 5 keV $^{20}Ne^{+}$ HS-LEIS spectra of the catalysts.

Comparison of the performance of various catalysts for the hydrogenation of benzaldehyde (or styrene)

The hydrogenation of styrene (or benzaldehyde) was used to evaluate the performance of the catalysts. The results are shown in Tables 1 and 2. In Table 1, the hydrogenation of benzaldehyde was carried out for 3 h under the reaction conditions (ethanol-10 ml; benzaldehyde-0.5 mL; reaction temperature-25 °C; hydrogen pressure-1.0 MPa), the yield of benzyl alcohol of Ni/C, Pt/Ni/C and Pd/Ni/C catalysts was <0.1%, 48% and 69%. 46% yield of benzyl alcohol can be obtained after the hydrogenation of benzaldehyde over the Pt-Pd/Ni/C catalyst for 0.5 h. The benzaldehyde hydrogenation rate catalyzed by Pt/Ni/C, Pd/Ni/C and Pt-Pd/Ni/C catalyst was 102 $mol_{benzaldehyde}$ $mol_{(Pt+Pd)}^{-1}$ h^{-1}, 80 $mol_{benzaldehyde}$ $mol_{(Pt+Pd)}^{-1}$ h^{-1} and 827 $mol_{benzaldehyde}$ $mol_{(Pt+Pd)}^{-1}$ h^{-1}, respectively. The results show that the Pt-Pd/Ni/C catalyst demonstrates the best catalytic performance for benzaldehyde hydrogenation. Table 2 gives the catalytic performance of each catalyst for the hydrogenation of styrene under the same reaction conditions (as shown in Table 2) , the catalytic performance of the catalysts are as follows: Pt-Pd/Ni/C (yield: 72.3%, hydrogenation rate: 5786 $mol_{styrene}$ $mol_{(Pt+Pd)}^{-1}$ h^{-1}) > Pt/Ni/C (yield: 64.0%, hydrogenation rate: 1212 $mol_{styrene}$ $mol_{(Pt+Pd)}^{-1}$ h^{-1}) > Pd/Ni/C (yield: 58.2%, hydrogenation rate: 1198 $mol_{styrene}$ $mol_{(Pt+Pd)}^{-1}$ h^{-1}) > Ni/C (yield< 0.1%). The above results show that the Pt-Pd/Ni/C catalyst is superior to Pt/Ni/C, Pd/Ni/C and Ni/C catalysts in the catalytic hydrogenation of styrene (or benzaldehyde). The reason is that the Pt-Pd/Ni/C catalyst possesses a unique nanostructure of “PtPd alloy nanoclusters on Ni nanoparticles”, and the synergistic effect between PtPd alloy nanoclusters and Ni nanoparticles enhances its catalytic hydrogenation performance. On the basis of the relevant literature and our previous works [43-45], the likely mechanism of the synergistic effect is given below: Hydrogen is preferentially absorbed and activated at Pt or Pd sites, forming activated hydrogen species (H*), benzaldehyde (or styrene) is activated at Ni sites, then H* is transferred to the Ni sites by a hydrogen spill-over effect (as a bridge), reacting with the activated benzaldehyde (or styrene), finally producing benzyl alcohol (ethylbenzene).

Table 1. Catalytic performance of the monometallic, bimetallic and trimetallic catalysts for benzaldehyde hydrogenation.[a]

Ent.	Catalyst (0.05 g)	t [b](h)	*r* [c]	Yield [d](%)
1	Ni/C	3	-	< 0.1
2	Pt/Ni/C	3	102	48
3	Pd/Ni/C	3	80	69
4	Pt-Pd/Ni/C	0.5	827	46

[a] reaction conditions: ethanol-10 ml, benzaldehyde-0.5 ml, H_2 pressure-1.0 MPa, reaction temperature-25 °C, [b] reaction time, [c] the unit of *r* is $mol_{benzaldehyde}$ $mol_{(Pt+Pd)}^{-1}$ h^{-1}, [d] yield to benzyl alcohol.

Table 2. Catalytic performance of monometallic, bimetallic and trimetallic catalysts for styrene hydrogenation.[a]

Ent.	Catalyst	t [b](h)	*r* [c]	Yield [d](%)
1	Ni/C (0.05 g)	18	-	< 0.1
2	Pt/Ni/C (0.05 g)	18	1212	64.0
3	Pd/Ni/C (0.025 g)	18	1198	58.2
4	Pt-Pd/Ni/C (0.025 g)	6	5786	72.3

[a] reaction conditions: ethanol-10 ml, styrene-0.5 ml, H_2 pressure-1.0 MPa, reaction temperature-25 °C, [b] reaction time, [c] the unit of *r* is $mol_{styrene}$ $mol_{(Pt+Pd)}^{-1}$ h^{-1}, [d] yield to ethylbenzene.

Effect of thermal-treatment temperature of Pt-Pd/Ni/C on its catalytic performance for the hydrogenation of benzaldehyde (or styrene)

In order to investigate the effect of thermal-treatment temperature on the catalytic performance of the Pt-Pd/Ni/C catalyst for the hydrogenation of benzaldehyde (or styrene), the Pt-Pd/Ni/C catalyst was calcined in H_2 at 200, 400 and 600°C for 2 h, respectively. Their catalytic performances are compared and the results are shown in Figure 10. It was found that the order of their catalytic activity was Pt-Pd/Ni/C-200 > Pt-Pd/Ni/C-400 > Pt-Pd/Ni/C-600 (particularly for styrene hydrogenation), indicating that the catalytic hydrogenation performance decreases with the increase of reducing treatment temperature of the Pt-Pd/Ni/C. The main reasons are as follows: (1) The size of Pt-Pd/Ni nanoparticles increases with the increase of annealing temperature; (2) the nanostructure of the Pt-Pd/Ni in the catalyst changes from “PtPd alloy nanoclusters on Ni nanoparticles” to “PtPdNi alloy nanoclusters on Ni nanoparticles”, the PtPd alloy can improve the catalytic hydrogenation performance of the catalyst and the nanostructure of “PtPd alloy nanoclusters on Ni nanoparticles” can generate the synergy effect of PtPd and Ni; (3) the content of precious metal on the surface of the catalyst decreases and thus the number of surface active sites for the adsorption and activation of H_2 at low temperature decreases.

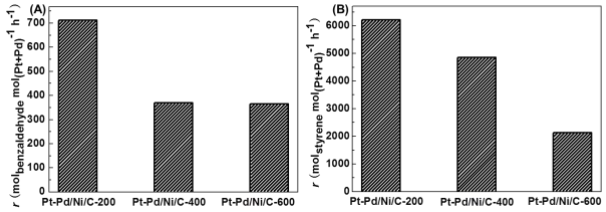

Figure 10. Catalytic performance of the Pt-Pd/Ni/C catalysts annealed at different temperatures for benzaldehyde (or styrene) hydrogenation: (A) reaction conditions: catalyst-0.05 g, ethanol-10 mL, benzaldehyde-0.5 mL, H_2 pressure-1.0 MPa, reaction temperature-25 °C; (B) reaction conditions: catalyst-0.025 g, ethanol-10 mL, styrene-0.5 mL, H_2 pressure-1.0 MPa, reaction temperature-25 °C.

Conclusions

A systematic study of the monometallic (Ni/C), bimetallic (Pt/Ni/C and Pd/Ni/C) and trimetallic (Pt-Pd/Ni/C) catalysts has been carried out to clarify the synergistic effect of multimetallic catalysis. Further thermal treatment of the Pt-Pd/Ni/C-X (X =200, 400 and 600°C) catalysts at a reducing H_2 atmosphere has modified the surface structure and chemistry. The as-synthesised trimetallic Pt-Pd/Ni/C catalyst possesses a nanostructure of relatively fine “PtPd alloy nanoclusters on Ni nanoparticles” (PtPd/Ni), and the Pt-Pd/Ni/C-600 catalyst show a nanostructure of relatively large “PtPdNi alloy cluster on Ni particles” (PtPdNi/Ni). The catalytic hydrogenation of benzaldehyde (or styrene), as model reaction systems, shows that the catalytic activity of the trimetallic systems is significantly higher than that of Pt/Ni/C, Pd/Ni/C and Ni/C catalyst, which is attributed to the formation of the nanostructure of “PtPd alloy nanoclusters on Ni nanoparticles” and the synergistic effect between the PtPd alloy nanoclusters and the Ni nanoparticles. With the increase of the thermal-treatment temperature, the catalytic hydrogenation performance is deteriorated because the resulting Pt-Pd/Ni nanostructure changes from “PtPd alloy nanoclusters on Ni nanoparticles”, fine and rich in noble elements, to “PtPdNi alloy clusters on Ni particles”, relatively coarse and lean in noble elements, and thus weak in synergistic effect between the PtPd alloy and Ni particles. The findings provide clear guidance for future development of multimetallic catalysts in similar systems.

Experimental Section

Synthesis of Ni/C

A pre-calculated amount of $Ni(NO_3)_2{\cdot}6H_2O$ was dissolved in a beaker with 200 mL ultrapure water and stirred vigorously for 10 minutes, then 0.5 g catalyst support (carbon black-BP-2000) was added and agitated for 1 h, to obtain the mixture. The beaker was then placed in a water bath to evaporate the water in the mixture at 80 °C. Then the as-obtained powder was placed in a blast oven and dried at 120 °C for 3 h. The powder was put into a quartz tube and then in a tube furnace, where it was reduced in hydrogen (99.999%) at 300 °C for 3 h. After the calcination, nitrogen was injected into the quartz tube, and then the temperature was brought down to ambient. The sample was recorded as Ni/C.

Synthesis of Pt/Ni/C, Pd/Ni/C, Pt-Pd/Ni/C

The Pt/Ni/C, Pd/Ni/C, Pt-Pd/Ni/C catalysts were prepared via galvanic replacement. Briefly, take the preparation process of Pt/Ni/C as an example, a certain amount of aqueous $H_2PtCl_6{\cdot}6H_2O$ solution (1.0 g $H_2PtCl_6{\cdot}6H_2O$/250 mL H_2O) was diluted with 200 mL ultrapure water and then put in a 250 ml conical bottle, 0.3 g Ni/C was added to the conical bottle and stirred for 4 h. The black solid was collected by filtration and washed several times with ultrapure water and absolute ethanol. The solid was dried in a vacuum oven at 60 °C for 6 h. The powder was reduced in hydrogen atmosphere at 300 °C for 2 h. After the reducing treatment, nitrogen was fed into the quartz tube until the temperature dropped to room temperature, and the Pt/Ni/C sample was obtained. The Pd/Ni/C and Pt-Pd/Ni/C catalysts were obtained via the same method and steps, the difference was that aqueous $H_2PtCl_6{\cdot}6H_2O$ solution was replaced with aqueous $PdCl_2$ solution (or the mixture of aqueous $H_2PtCl_6{\cdot}6H_2O$ and $PdCl_2$ mxiture).

The as-obtained Pt-Pd/Ni/C catalyst was packed into a quartz tube and reduced in hydrogen atmosphere at 200, 400 and 600 °C, respectively for 2 h. The catalysts were labelled as Pt-Pd/Ni/C-200, Pt-Pd/Ni/C-400 and Pt-Pd/Ni/C-600, respectively.

Inductively coupled plasma mass spectrometry (ICP-MS) technique was used to determine the metal contents in the catalysts: Pt/Ni/C: Pt-2.15 wt%, Ni-14.8 wt%; Pd/Ni/C: Pd-2.07 wt%, Ni-15.2 wt%; Pt-Pd/Ni/C (containing Pt-Pd/Ni/C-200, Pt-Pd/Ni/C-400 and Pt-Pt/Ni/C-600): Pt-1.1 wt%, Pd-1.0 wt%, Ni-14.9 wt%.

Characterization of the catalysts

All X-ray diffraction (XRD) measurements were performed on Rigaku Ultima IV X-ray diffractometer. Cu *Ka* (0.15406 nm) is the X-ray source, the operating voltage is 40 kV, the current is 30 mA. The scanning angle (2**θ**) was 10°~90°. The XRD patterns were analyzed using Jade software. X-ray photoelectron spectroscopy (XPS) was used to analyze the chemical states and contents of the elements on the surface of the samples. PHI-Quantum 2000, Al *Ka* (hv = 1486.6 eV) was used as the X-ray source. Transmission electron microscope (TEM), high resolution TEM (HRTEM) and scanning transmission electron microscopy energy dispersive X-ray spectroscopy (STEM-EDS) elemental mapping and line-scanning analysis of the catalysts were performed on FEI TECNAI F30. The accelerating voltage was 300 kV. The sample to be tested was dispersed in anhydrous ethanol and ultrasonic dispersion, and then a few drops were attached to the copper grid. High-sensitivity low-energy ion scattering (HS-LEIS) was used to analyze the surface atomic species and composition of the catalyst. The instrument was IonTOF Qtac100, the initial kinetic energy was 5 keV with $^{20}Ne^+$ ions beam as sputtering source, the sample current was 1.6 nA. The catalyst was calcined in a muffle furnace at 800 °C for 3 h to remove the support carbon. And the residual solid was dissolved in aqua regia. The metallic elements in the catalysts were determined using Agilent ICP-MS 4500-300 inductively coupled plasma.

Catalytic performance evaluation of the catalysts

The catalytic hydrogenation of benzaldehyde (or styrene) was used as a model reaction to evaluate the catalytic performance of the catalysts. The reaction was carried out in a high-pressure reactor (Parr 4848) under the following conditions: Hydrogen pressure-1.0 MPa, reaction temperature-25 °C, reaction solvent-10 mL ethanol, reaction substrate-0.5 mL benzaldehyde or styrene, catalyst-0.05 g or 0.025 g, stirring rate-500 r min^{-1}. After the reaction was complete, an exhaust valve was opened to vent the remaining gas from the reaction kettle. And the catalyst was separated from the reaction liquid by centrifugation. Shimadzu gas chromatography (GC 2010) and gas chromatography-mass

spectrometry (GC-MS 2010) were used to analyze the liquid products.

Acknowledgements

This research was supported by the National Natural Science Foundation of China (Grant No. 21763011), Research Fund Program of Key Laboratory of Fuel Cell Technology of Guangdong Province, Guangdong Provincial Key R&D Program (No. 2020B0101370003), HKU Start-Up Fund and HK Scholars Program.

Keywords: Pt-Pd/Ni/C • annealing temperature • trimetallic catalyst • hydrogenation • nanostructure

[1] D. M. Alonso, S. G. Wettstein, J. A. Dumesic, *Chem. Soc. Rev.* **2012**, *41*, 8075-8098.
[2] Xu J, White T, Li P, J. Yu, W. Yuan, Y.-F. Han, *J. Am. Chem. Soc.* **2010**, *132*, 10398-10406.
[3] X. Lan, K. Xue, T. Wang, *J. Catal.* **2019**, *372*, 49-60.
[4] M. Chen, D. Kumar, C.-W. Yi, D. W. Goodman, *Science* **2005**, *310*, 291-293.
[5] D. I. Enache, J. K. Edwards, P. Landon, B. Solsona-Espriu, A. F. Carley, A. A. Herzing, M. Watanabe, C. J. Kiely, D. W. Knight, G. J. Hutchings, *Science* **2006**, *311*, 362-365.
[6] H. Liu, R. Fang, Z. Li, Y. Li, *Chem. Eng. Sci.* **2015**, *122*, 350-359.
[7] Y. Huang, Y. Ma, Y. Cheng, L. Wang, X. Li, *Catal. Comm.* **2015**, *69*, 55-58.
[8] Y. Huang, Y. Ma, Y. Cheng, L. Wang, X. Li, *Ind. Eng. Chem. Res.* **2014**, *53*, 4604-4613.
[9] M. O. Haus, A. Meledin, S. Leiting, Y. Louven, N. C. Roubicek, S. Moos, C. Weidenthaler, T. E. Weirich, R. Palkovits, *ACS Catal.* **2021**, doi: 10.1021/acscatal.0c05612.
[10] J. Su, W. Shi, X. Liu, L. Zhang, S. Cheng, Y. Zhang, G. A. Botton, B. Zhang, *J. Catal.* **2020**, *388*, 164-170.
[11] M. H. Ab Rahim, M. M. Forde, R. L. Jenkins, C. Hammond, Q. He, N. Dimitratos, J. A. Lopez-Sanchez, A. F. Carley, S. H. Taylor, D. J. Willock, *Angew. Chem. Int. Ed.* **2013**, *52*, 1280-1284.
[12] L. Kesavan, R. Tiruvalam, M. H. Ab Rahim, M. I. bin Saiman, D. I. Enache, R. L. Jenkins, N. Dimitratos, J. A. Lopez-Sanchez, S. H. Taylor, D. W. Knight, C. J. Kiely, G. J. Hutchings, *Science* **2011**, *331*, 195-199.
[13] G. Chen, Y. Zhao, G. Fu, P. N. Duchesne, L. Gu, Y. Zheng, X. Weng, M. Chen, P. Zhang, C.-W. Pao, J.-F. Lee, N. Zheng, *Science* **2014**, *344*, 495-499.
[14] L. Yang, S. Shan, R. Loukrakpam, V. Petkov, Y. Ren, B. N. Wanjala, M. H. Engelhard, J. Luo, J. Yin, Y. Chen, C.-J. Zhong, *J. Am. Chem. Soc.* **2012**, *134*, 15048-15060.
[15] S.-M. Hwang, S. J. Han, H.-G. Park, H. Lee, K. An, K.-W. Jun, S. K. Kim, *ACS Catal.* **2021**, *11*, 2267-2278.
[16] M. Gholinejad, F. Khosravi, M. Afrasi, J. M. Sansano, C. Nájera, *Catal. Sci. Technol.* **2021**, doi.org/10.1039/D0CY02339F.
[17] W. Zhang, H. Xin, Y. Zhang, X. Jin, P. Wu, W. Xie, X. Li, *J. Catal.* **2021**, *395*, 375-386.
[18] L. Ning, M. Zhang, S. Liao, Y. Zhang, D. Jia, Y. Yan, W. Gu, X. Liu, *ChemCatChem* **2021**, *13*, 704-711.
[19] D. Yanase, T. Hara, F. Sato, Y. Yamada, S. Sato, *Appl. Catal. A: Gen.* **2021**, *616*, 118093.
[20] F. Sperner, W. Hohmann, *Platinum Met. Rev.* **1976**, *20*, 12-20.
[21] C. Mohr, H. Hofmeister, P. Claus, *J. Catal.* **2003**, *213*, 86-94.
[22] C. Mohr, H. Hofmeister, J. Radnik, P. Claus, *J. Am. Chem. Soc.* **2003**, *125*, 1905-1911.
[23] L. Zhu, S. Shan, V. Petkov, W. Hu, A. Kroner, J. Zheng, C.Yu, N. Zhang, Y. Li, R. Luque, C.-J. Zhong, H. Ye, Z. Yang, B. H. Chen, *J. Mater. Chem. A* **2017**, *5*, 7869-7875.
[24] P. Paalanen, B. M. Weckhuysen, M. Sankar, *Catal. Sci. Technol.* **2013**, *3*, 2869-2880.
[25] R. Ferrando, J. Jellinek, R. L. Johnston, *Chem. Rev.* **2008**, *108*, 845-910.
[26] B. Huang, Y. He, Y. Zhu, Z. Wang, K. Cen, *Langmuir* **2020**, *36*, 3111-3118.
[27] R. Wu, Y. Li, W. Gong, P. K. Shen, *ACS Sustainable Chem. Eng.* **2019**, *7*, 8419-8428.
[28] S. Alayoglu, A. U. Nilekar, M. Mavrikakis, B. Eichhorn, *Nat. Mater.* **2008**, *7*, 333-338.
[29] B. N. Wanjala, J. Luo, R. Loukrakpam, B. Fang, D. Mott, P. N. Njoki, M. Engelhard, H. R. Naslund, J. K. Wu, L. Wang, O. Malis, C.-J. Zhong, *Chem. Mater.* **2010**, *22*, 4282-4294.
[30] L. Zhu, H. Zhang, L. Zhong, J. Zheng, C. Yu, N. Zhang, B. H. Chen, *Fuel* **2018**, *216*, 208-217.
[31] L. Zhu, M. Cao, L. Li, H. Sun, Y. Tang, N. Zhang, J. Zheng, H. Zhou, Y. Li, L. Yang, C.-J. Zhong, B. H. Chen, *ChemCatChem* **2014**, *6*, 2039-2046.
[32] L. Liao, L. Chen, R.-P. Ye, X. Tang, J. Liu, *Chem. Asian J.* **2021**, *16*, 678-689.
[33] B. Wei, H. Yang, H. Hu, D. Wang, L. Jin, *Fuel* **2020**, *279*, 118533.
[34] L. Yang, Y. Wang, H. Feng, H. Zeng, C. Tan, J. Yao, J. Zhang, L. Jiang, Y. Sun, *Chem. Asian J.* **2021**, *16*, 34-38.
[35] L. Shen, J. Ying, G. Tian, M. Jia, X.-Y. Yang, *Chem. Asian J.* **2021**, doi.org/10.1002/asia.202100156.
[36] Y. Yu, Y. Gong, B. Cao, H. Liu, X. Zhang, X. Han, S. Lu, X. Cao, H. Gu, *Chem. Asian J.* **2021**, *16*, 837-844.
[37] Y. Hao, X. Wang, Y. Zheng, J. Shen, J. Yuan, A. Wang, L. Niu, S. Huang, *Int. J. Hydrogen Energy* **2016**, *41*, 9303-9311.
[38] B. Chen, F. Li, Z. Huang, G. Yuan, *Appl. Catal. A: Gen.* **2015**, *500*, 23-29.
[39] H. Xu, Z. Shen, G. Chen, C. Yin, Y. Liu, Z. Ge, Y. Wang, Z. Zheng, X. Li, *Fuel* **2020**, *275*, 118036.
[40] D. Wang, Y. Zhu, *J. Chem.* **2018**, *2018*, 1-7.
[41] Z. Guo, Y. Chen, L. Li, X. Wang, G. L. Haller, Y. Yang, *J. Catal.* **2010**, *276*, 314-326.
[42] W. Liu, Q. Tian, J. Yang, Y. Zhou, H. Chang, W. Cui, Q. Xu, *Chem. Asian J.* **2021**, doi.org/10.1002/asia.202100239.
[43] R. Prins, *Chem. Rev.* **2012**, *112*, 2714-2738.
[44] L. Zhu, H. Zhang, N. Ma, C. Yu, N. Ding, J.-L. Chen, C.-W. Pao, J.-F. Lee, Q. Xiao, B. H. Chen, *J. Catal.* **2019**, *377*, 299-308.
[45] W. Karim, C. Spreafico, A. Kleibert, J. Gobrecht, J. VandeVondele, Y. Ekinci, J. A. van Bokhoven, *Nature* **2017**, *541*, 68-71.

Entry for the Table of Contents

FULL PAPER

Trimetallic Pt-Pd-Ni catalysts were successfully designed, synthesized and/or further heat-treated: the as-synthesized catalyst is characterised by fine “PtPd alloy nanoclusters on Ni nanoparticles”, whereas that after further treatment shows a structure of “PtPdNi alloy clusters on Ni particles”. The former yields much superior catalytic performance for benzaldehyde (styrene) hydrogenation at room temperature due to the synergistic effect of PtPd and Ni.

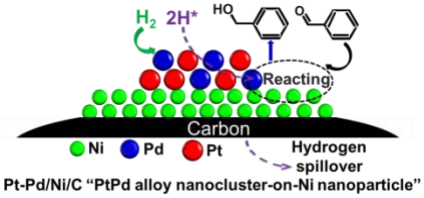

Pt-Pd/Ni/C “PtPd alloy nanocluster-on-Ni nanoparticle”

Tuo Zheng,[b] Fengshun Wu,[b] Huan Fu,[b] Li Zeng,[b] Congxiao Shang,[a, c] Lihua Zhu,[a, b] and Zhengxiao Guo*[a, c]*

Page No. – Page No.

Rational design of Pt-Pd-Ni trimetallic nanocatalysts for room temperature styrene and benzaldehyde hydrogenation